A Digital Simulation of Transient Oxygen Transport in Capillary-Tissue Systems (Cerebral Grey Matter)

Development of a Numerical Method for Solution of Transport Equations Describing Coupled Convection-Diffusion Systems.

DANIEL D. RENEAU, JR. and DUANE F. BRULEY

Clemson University, Clemson, South Carolina

and MELVIN H. KNISELY

Medical College, Charleston, South Carolina

The mechanism by which oxygen is transported from capillaries into tissue for cell respiration has been a subject of interest since the work of August Krogh in 1919. Mathematical analyses of the diffusion process have been obtained by several investigators (11, 12, 18), but are limited in scope by the complicated nature of the problem. However, the solutions that exist give enough insight to inspire a more rigorous treatment. With the advent of electronic computers more complete analyses are now within reach (16).

The human brain accounts for less than 4% of the total body weight, yet it uses 15 to 20% of the total body oxygen consumption. This high metabolic rate makes the brain particularly vulnerable to any change in the normal oxygen supply. The fact that following a cessation of cerebral blood flow, unconsciousness develops within 10 sec., and irreversible damage within 10 min., demonstrates the importance of understanding the dynamics of oxygen supply to the brain.*

The purpose of this work is to obtain a better understanding of transient oxygen release, diffusion and consumption in the capillaries and tissue of cerebral grey matter by describing the different aspects of the convection-diffusion system in a mathematical model. Insight into the problem can be gained by the formulation and solution of a detailed mathematical model.

ANATOMY

To approach mathematical modeling of a diffusion process from a deterministic point of view, the physical dimensions and shape of the system must be defined. The majority of previous mathematical work concerning oxygen diffusion in living tissue used the Krogh capillary cylinder arrangement as the physical geometry (Figure 1). August Krogh (*13*) developed the concept after observing the anatomy of capillaries in striated muscle. Krogh found that in a given portion of muscle the capillaries were dispersed with conspicuous regularity. Consequently, a single capillary and the tissue surrounding it could be extracted and treated as a representative sample of the whole (Figure 2).

Although Krogh and later investigators studied the mathematics of oxygen supply in skeletal muscle and other organs, relatively few similar publications exist regarding oxygen supply to the nerve cells of the brain. The apparent arrangement of capillaries in cerebral tissue might make one question the concept of a homogeneous geometry. However, in 1950 Opitz and Schneider (*14*) showed how the homogeneous Krogh arrangement of tissue and capillaries could be extended to cerebral grey matter. Special equations based on experimental histological data were developed to calculate the radius of supply of individual capillaries. Later, Thews (*20*) perfected the equations of Opitz and Schneider and calculated the diffusion distance, based on a hexagonal geometry, to be 30μ as the radius of the region supplied by a single capillary in human grey matter. The diameter of cerebral capillaries was given as 5 to 6μ.

The cells least supplied with oxygen are located on the periphery of the tissue cylinder radially adjacent to the venous end of the capillary. This position, named by Becker, is referred to in the literature as the *lethal corner* (*14, 20*).

A more detailed account of the above historical development is given in Reneau, Bruley, and Knisely (*16*).

PHYSIOLOGY

A very small percentage of oxygen, normally 1% or less, is present in blood plasma as physically dissolved oxygen. The remainder is combined with the hemoglobin of erythrocytes. The reaction between oxygen and hemoglobin is so fast that many investigators have been unable to obtain a rigorous kinetic model. It has been reported that in the lung under normal conditions the half time of change of hemoglobin from the deoxygenated state to the oxygenated state is 0.01 sec. or less (3). The equilibrium relationship between dissolved oxygen and chemically combined oxygen is shown in the oxygen dissociation curve (Figure 3).

As blood flows through a capillary in brain from arterial

Daniel D, Reneau, Jr. is with the Louisiana Polytechnic Institute, Ruston, Louisiana.

to venous end, dissolved oxygen in the plasma diffuses to tissue cells and is replenished by oxygen released from hemoglobin. Under normal conditions blood entering the brain has an oxygen content of 20 vol. % (volume of oxygen per 100 vol. of blood) and a partial pressure of 95 mm. Hg. Blood leaving the brain has an oxygen partial pressure of 34 mm. Hg. (*14*).

After diffusing from the capillary through the capillary wall and into tissue, oxygen is metabolized by nerve cells. In a review of cerebral oxygen supply, Opitz and Schneider (*14*) reported that the oxygen consumption of the brain was relatively uniform with little variation from periods of maximum brain activity to periods of complete rest. Oxygen consumption of the total brain is generally accepted as 3.4×10^{-2} cc. oxygen/100 g. min. Opitz and Schneider used a 5/1 respiration ratio of grey to white matter and a 6/4 weight ratio to calculate 5.0×10^{-2} cc. oxygen/100 g. min. as the oxygen consumption of grey matter.

The rate at which oxygen is supplied to nerve cells for metabolism is dependent on the permeability of blood and tissue. The diffusion coefficient for oxygen in erythrocytes is not the same as in plasma. However, Thews (*20*) suggests that 1.75×10^{-5} cc. oxygen/cm. min. atm. (1.12×10^{-5} sq.cm./sec.) at 37°C. can be used without introducing significant error. Thews (*20*) also experimentally determined a diffusion coefficient for oxygen in grey matter and reported this value as 1.70×10^{-5} sq.cm./sec. at 37°C.

DERIVATION OF EQUATIONS

In developing equations to describe the conditions associated with oxygen transport in cerebral grey matter the following assumptions were used. (References are given to indicate precedence.)

1. The Krogh capillary-tissue arrangement may be used when the radius of the region of supply is determined by the method of Thews (*20*).
2. The time of reaction for the rate of release of oxygen from erythrocytes is negligible compared to the time required for diffusion to nerve cells (*20*). Consequently, chemical equilibrium exists in the capillary between dissolved oxygen and oxyhemoglobin, and the oxygen dissociation curve (Figure 3) can serve to represent this relationship as blood flows through the capillary.
3. Oxygen released from erythrocytes over a small axial section is assumed to be distributed over the section (plasma and erythrocytes) as if the release had occurred at all points. In actual flow conditions, hemoglobin is contained within erythrocytes and cannot be distributed homogeneously. The dispersion of erythrocytes in plasma is not necessarily homogeneous and varies from region to region. In addition the width of plasma gaps between erythrocytes may vary. Assumption 3 idealizes the above phenomena to allow mathematical modeling in a distributed parameter manner.
4. The capillary wall offers a negligible resistance to the diffusion of oxygen (*12, 14, 20*). The oxygen concentration curve at the interface is continuous, and oxygen transport across the interface can be described by Fick's first law.
5. A type of creeping flow is assumed to exist in the capillary. This is substantiated by the investigations of others (*21*).
6. A flat velocity profile is assumed. Bloch (*4*) has photographed the flow of blood through the microcirculation at rates up to 3,000 frames/sec. which shows that erythrocytes flow single file through capillaries. The diameter of erythrocytes is approximately equal to the internal diameter of the capillary which would tend to produce a flat velocity profile.
7. The difference in the rates of diffusion of oxygen through plasma and erythrocytes is accounted for by the use of an overall diffusion coefficient selected from the work of Thews (*20*).
8. The brain cells are distributed homogeneously in the tissue cylinder (*5, 12, 14*).
9. Cell metabolism is constant (*14, 20*), physical properties are constant, blood flow is in the X direction only (arteriole to capillary to venule), and the system is axially symmetric.

On the basis of the assumptions, a mathematical model was developed to describe the related transport processes. The model consists of four equations, one each for the capillary and tissue and two for the interface. The equations are coupled, nonlinear, partial differential equations with three independent variables. The derivation will be covered briefly here, but a detailed derivation may be found in Reneau, Bruley, and Kinsely (*16*), or Reneau (*17*).

The equation for the capillary takes the form,

$$\frac{\partial P}{\partial t} = D_1 \left[\frac{\partial^2 P}{\partial r^2} + \frac{1}{r} \frac{\partial P}{\partial r} \right] + D_1 \frac{\partial^2 P}{\partial X^2} - V \frac{\partial P}{\partial X} - \frac{VN}{C_1} \frac{\partial \Psi}{\partial X} \quad (1)$$

Ψ is a function of the oxygen partial pressure of plasma and of carbon dioxide partial pressure. Changes in carbon dioxide produce changes in the oxygen dissociation curve (Figure 3). However, the percent saturation of erythrocytes with oxygen can be obtained through use of the following equation (*19*):

$$\Psi = \frac{k P^n}{1 + kP^n} \quad (2)$$

Incorporation of Equation (2) into Equation (1) yields a more functional capillary equation (*16*).

$$\frac{\partial P}{\partial t} = D_1 \left[\frac{\partial^2 P}{\partial r^2} + \frac{1}{r} \frac{\partial P}{\partial r} \right] + D_1 \frac{\partial^2 P}{\partial X^2} - V \frac{\partial P}{\partial X} - \left[\frac{VNk\eta P^{n-1}}{C_1 (1 + kP^n)^2} \right] \frac{\partial P}{\partial X} \quad (3)$$

The equations for the blood-tissue interface are,

$$P_i|_{\text{blood}} = P_i|_{\text{tissue}} \quad (4)$$

$$D_1 C_1 \frac{\partial P}{\partial r} \Bigg|_{\substack{r=R_1 \\ \text{blood}}} = D_2 C_2 \frac{\partial P}{\partial r} \Bigg|_{\substack{r=R_1 \\ \text{tissue}}} \quad (5)$$

The tissue equation is,

$$\frac{\partial P}{\partial t} = D_2 \left[\frac{\partial^2 P}{\partial r^2} + \frac{1}{r} \frac{\partial P}{\partial r} \right] + D_2 \frac{\partial^2 P}{\partial X^2} - \frac{A}{C_2} \quad (6)$$

Boundary Conditions

Initial and boundary conditions imposed on the model were as follows: (For location of positions refer to grid work given in Figure 4)

initial condition

$P(x, r, 0)$ = solution from steady state equations (*16*).

boundary condition 1

$P(0, r, t)$ = given step change $t > 0$, $j \leq J - 1$

boundary condition 2

$$\frac{\partial P}{\partial X} = 0 \quad X = 0; \quad J + 1 \leq j \leq K; \quad t > 0$$

boundary condition 3

$$\frac{\partial P}{\partial r} = 0 \quad r = 0; \quad \text{for all } i \text{ and } t$$

boundary condition 4

$$\frac{\partial P}{\partial r} = 0 \quad r = R_2; \text{ for all } i \text{ and } t$$

boundary condition 5

$$\frac{\partial P}{\partial X} = m \quad X = L; \quad \text{for all } j \text{ and } t$$

The difference between boundary condition 1 and boundary condition 2 is readily understood by recognizing that a change in input concentration occurs only in the capillary (boundary condition 1) and not in the tissue (boundary condition 2). The proper gradient for use at the venous end of the capillary (boundary condition 5) was selected carefully. In the actual capillary pattern of the brain a zero gradient did not appear to completely describe the system. On the other hand, the gradient established by steady state solution (*16*) offered the best possibilities for studying the effect of axial diffusion. On this basis, m, was chosen for the present studies, and the solution technique was adapted to fit any specified gradient.

Validity of Assumptions

Considering valid assumptions, the criteria of performance of any mathematical model is the ability of the model to match experimental data. The amount of experimental data available concerning oxygen partial pressures in the grey matter of the brain is scarce and at present difficult to obtain through experimental means. The only exact experimental data available is steady state arterial oxygen partial pressures vs. corresponding venous oxygen partial pressures.

Steady state solutions of Equations (3) through (6) were the subject of a previous publication (*16*). In that paper comparisons were given between numerical solutions and experimental measurements. Various arterial oxygen partial pressures and associated velocity changes were used as input data for the equations. Venous oxygen partial pressures were calculated and compared with corresponding experimental venous values. Numerical values agreed within 2% of experimental values (Figure 5, upper curve).

Another test was conducted for the case in which the acidity of the blood was changed by allowing the partial pressure of carbon dioxide to change from 40 to 20 mm. Hg. In this state of hypocapnia several changes occur including a large shift of the oxygen dissociation curve (Figure 3) and deviations from the normal flow rate. By using given experimental data for arterial conditions (*14*), a series of calculations were conducted to determine venous conditions. A comparison of experimental and numerical results are shown in Figure 5 (lower curve). As can be seen, agreement was very good.

To check the assumption of plug flow, the effect of velocity profile on the diffusion of oxygen from the capillary to tissue was investigated by solving the equations (steady state) for the case of a parabolic velocity profile. A comparison of the results is shown in Figure 6. The changes in both radial and axial partial pressure profiles were negligible.

The results shown here tend to give increased confidence in the accuracy of the model and the validity of the assumptions. After introducing a rather drastic step change in arteriole oxygen content, the transient model solution converged to the final state values as calculated by the steady state model.

DEVELOPMENT OF NUMERICAL ANALYSIS METHOD FOR CONVECTION-DIFFUSION SYSTEMS

The numerical solution techniques developed in this section are not limited to this particular problem. The method is applicable to any coupled convection-diffusion system in which streamline flow characterizes the fluid motion, a negligible resistance is present at the solid-liquid interface, and the system is axially symmetric. The method may be applied to both linear and nonlinear equations and to heat as well as mass transfer. A change in boundary conditions from the ones given does not affect the utility of the technique.

Stability limitations did not allow complete explicit differencing. The equations could have been implicitly differenced in a manner similar to steady state parabolic equations (*16*). However, such treatment would result in simultaneous algebraic equations of form similar to differenced elliptic equations, and require iterative solution methods for each time increment. A knowledge of the computer time required for a single steady state solution by iteration eliminated this method. Also, since it was necessary to study axial diffusion, the numerical solution shift method of Bailey and Gogarty (*2*) was not applicable.

Peaceman and Rachford (*15*), and also Douglas (*9*), developed an alternating-direction implicit procedure to describe unsteady state diffusion in two directions. Later, Brian (*6*) supplemented the work by expanding the procedure to describe unsteady state diffusion in three directions. Recently, Ananthakrishnan, Gill, and Barduhn (*1*) modified the Peaceman-Rachford method to describe unsteady state two-dimensional diffusion in laminar flow systems.

For three reasons, direct use of a single alternating-direction implicit method to solve the present problem was not possible.

1. Two different diffusion systems were involved, yet each depended on conditions existing in the other.
2. The interface equations contained derivatives with respect only to radial distance. Therefore, it was difficult to meet the requirements of an alternating direction method when only one direction was involved.
3. The capillary equation was nonlinear.

The numerical method developed here is a combination of the original Peaceman-Rachford technique and the modified Peaceman-Rachford technique. First, the x-derivatives of the tissue and capillary equations are implicitly differenced and the r-derivatives explicitly differenced. The resulting equations are of a form easily solved by the method of Thomas (*7*). Second, the r-derivatives of each equation are implicitly differenced and the x-derivatives explicitly differenced. These equations are also solvable by the method of Thomas. The tissue and capillary equations are linked by the interface equations which are adapted to the implicit scheme by alternately applying them in two different ways. A special equation is used to generate an approximate value for the nonlinear coefficient. Solution then proceeds by alternating between the x-implicit equations and r-implicit equations for successive time steps.

Alternating Direction Technique: X-Implicit Equation for the Capillary

Rewriting Equation (3) in a more appropriate form yields,

$$\frac{\partial P}{\partial t} + K\frac{\partial P}{\partial x} = D_1\left[\frac{\partial^2 P}{\partial r^2} + \frac{1}{r}\frac{\partial P}{\partial r}\right] + D_1\frac{\partial^2 P}{\partial x^2} \quad (7)$$

where,

$$K = v\left[1 + \frac{\eta N k P^{\eta-1}}{c_1(1 + kP^{\eta})^2}\right]$$

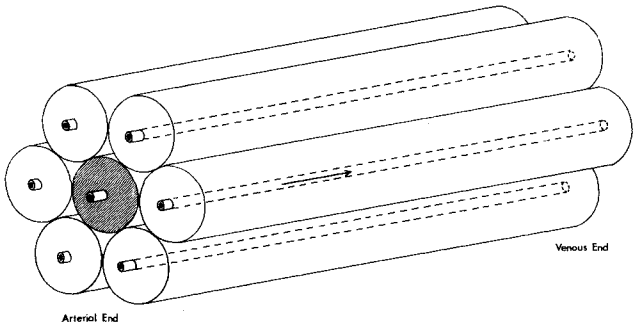

Fig. 1. Krogh tissue cylinder arrangement.

The x-derivatives may be replaced with an implicit formulation and the r-derivatives with an explicit formulation as follows: (see Figure 4)

$$\left[\frac{\partial P}{\partial t}\right]_{j,i,2n+1} = \frac{P_{j,i,2n+1} - P_{j,i,2n}}{e}$$

$$\left[K\frac{\partial P}{\partial x}\right]_{j,i,2n+1} = K_{j,i,2n+1}\left[\frac{P_{j,i+1,2n+1} - P_{j,i+1,2n+1}}{2k}\right]$$

$$\left[D_1\frac{\partial^2 P}{\partial x^2}\right]_{j,i,2n+1} = D_1\left[\frac{P_{j,i+1,2n+1} - 2P_{j,i,2n+1} + P_{j,i-1,2n+1}}{k^2}\right]$$

$$D_1\left[\frac{1}{r}\frac{\partial P}{\partial r}\right]_{j,i,2n} = \frac{D_1}{r}\left[\frac{P_{j+1,i,2n} - P_{j-1,i,2n}}{2h_1}\right]$$

$$D_1\left[\frac{\partial^2 P}{\partial r^2}\right]_{j,i,2n} = D_1\left[\frac{P_{j+1,i,2n} - 2P_{j,i,2n} + P_{j-1,i,2n}}{h_1{}^2}\right]$$

where,

j indexes radial distance

i indexes axial distance

$(2n + 1)$ indexes unknown time level

$2n$ indexes known time level

$n = 0, 1, 2 \ldots$

The time index $2n$, $2n + 1$ and, later, $2n + 2$ are in accordance with the alternating-direction technique. A single value of n is used twice before it is incremented, first for the x-implicit set of equations in which $2n + 1$ is the unknown time level and $2n$ is the known time level, and secondly in the r-implicit set of equations in which $2n + 2$ is the unknown and $2n + 1$ is the known. This will become clear as the differenced equations in this section develop. For a more complete discussion on the alternating-direction differencing forms see the work of Peaceman and Rachford (*15*) or Ananthakrishnam, Gill, and Barduhn (*1*).

By substituting the above forms into Equation (7), collecting terms, and rearranging yields*,

$$F_i P_{j,i+1,2n+1} + G_i P_{j,i,2n+1} + H_i P_{j,i-1,2n+1} = Z_i \quad (8)$$

where,

$$i = 2, 3, 4 \ldots I - 1$$

$$j = 2, 3, 4 \ldots J - 1$$

$$K = K_{j,i,2n+1} = v\left[1 + \frac{NknP^{n-1}{}_{j,i,2n+1}}{c_1(1 + kP^{n}{}_{j,i,2n+1})^2}\right]$$

In order to use Equation (8) the term $K_{j,i,2n+1}$ must be evaluated, but $K_{j,i,2n+1}$ involves the unknown term $P_{j,i,2n+1}$. An estimation technique similar to the method used in the previous study (*16*) was used to generate an approximation of the variable. The method is analogous to the one suggested by Douglas (*10*) for determining a nonlinear source term. For a nonlinear term resulting from a coefficient of a derivative this estimation procedure could lead to a serious stability limitation. However, since satisfactory results were obtained in the previous problem, the method was applied to the transient equation.

Thus,

$$P_{j,i,2n+1} = P_{j,i,2n} + e\left|\frac{\partial P}{\partial t}\right|_{j,i,2n} \quad (9)$$

The time derivative was evaluated by placing an explicit difference for time level $2n$ on the right hand side of Equation (3).

The coefficients F, G, and H necessary for the solution of Equation (8) were evaluated with use of Equation (9). The Z constants were evaluated from values of the dependent variable at known time level $2n$ and with use of fictitious boundaries for $j = 2$.

The boundary condition for the venous end of the capillary, $\left.\frac{\partial P}{\partial x}\right|_{i=I} = m$, was treated in the same special manner and for the same reasons as previously outlined (*16*), or,

$$P_{j,I,2n+1} - P_{j,I-1,2n+1} = Z_I \quad (10)$$

where,

$$i = I$$

$$j = 1, 2, 3, \ldots J - 1, J, J + 1, \ldots K - 1, K$$

and,

$$Z_I = mk$$

Boundary Condition 1 states that the magnitude of the step change is a constant for all times; therefore,

$$P_{j,1,2n+1} = P_{j,1} \quad (11)$$

If we let,

$$P_i = P_{j,i,2n+1}$$
$$P_{i+1} = P_{j,i+1,2n+1}$$
$$P_{i-1} = P_{j,i-1,2n+1} \quad (12)$$

and apply Equations (8), (10), and (11) to the capillary, the following set of simultaneous equations result for each j column.

$$\begin{aligned} G_2P_2 + F_2P_3 &= Z_2 + H_2P_1 && i = 2 \\ H_iP_{i-1} + G_iP_i + F_iP_{i+1} &= Z_i && 3 \leq i \leq I - 1 \\ -P_{I-1} + P_I &= Z_I && i = I \end{aligned} \quad (13)$$

These equations may be solved in an easy manner by the aforementioned method of Thomas (*7*).

Equation set (13) may be applied to each j column within the range $2 \leq j \leq J - 1$.

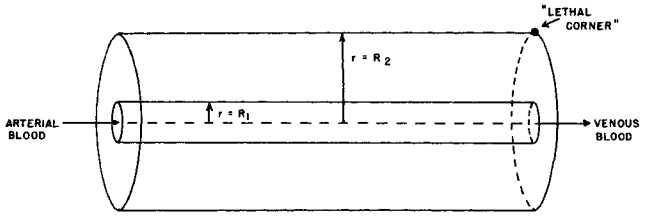

Fig. 2. Krogh tissue cylinder.

Alternating Direction Technique: X-Implicit Equation for the Tissue

Equation (6) applies to all tissue positions bounded by $J + 1 \leq j \leq K$ and $1 \leq i \leq I - 1$. The X-implicit technique replaced the derivatives in the same manner as in the capillary equation. After the differenced terms were

* Functional forms for the constants F, G, . . . etc., in this and the following equations can be obtained by the direct substitution indicated. However, a more detailed step-by-step mathematical description can be obtained from the authors.

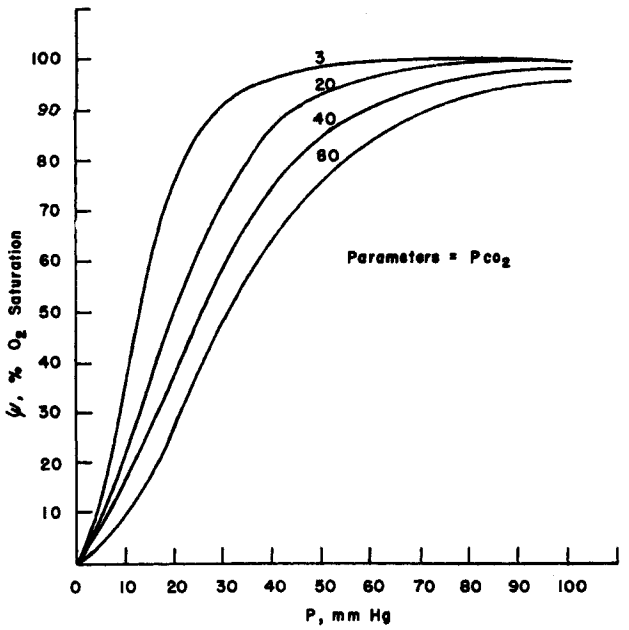

Fig. 3. Oxygen dissociation curve of human blood.

substituted, collected, and rearranged, the following algebraic equation was obtained:

$$FF_iP_{j,i+1,2n+1} + GG_iP_{j,i,2n+1} + HH_iP_{j,i-1,2n+1} = ZZ_i \tag{14}$$

where,

$$j = J+1,\ J+2,\ \ldots.\ K$$

$$i = 1, 2, 3, \ldots.\ I-1$$

GG, FF, and HH are constants at all positions for a given set of conditions, and with use of boundary condition 4 the Z's may be calculated from known values of the dependent variable at time level $2n$.

In accordance with boundary condition 2, a special equation may be written for the $X = 0$ position; or,

$$P_{j,i-1,2n+1} = P_{j,i+1,2n+1} \qquad i = 1 \tag{15}$$

The following set of equations result for each j column by substituting Equation (15) into Equation (14) applying Equation (10) to position $i = I$, and using the nomenclature established in Equation (12):

$$\begin{aligned} GG_1P_1 + (FF_1 + HH_1)P_2 &= Z_1 && i = 1 \\ HH_iP_{i-1} + GG_iP_i + FF_iP_{i+1} &= Z_i && 2 \leq i \leq I-1 \\ -P_{I-1} + P_I &= Z_I && i = I \end{aligned} \tag{16}$$

Equation set (16) can be solved by the method of Thomas for each j column within the range $J+1 \leq j \leq K$.

Interface Equation for Use with X-Implicit Capillary and Tissue Equations

Equation sets (13) and (16) allow calculation of all columns in Figure 4 except column J. Once the $J-1$ and $J+1$ columns are evaluated at time level $2n+1$, the J column may be determined by manipulation of the interface equations. If a backward difference is applied to the left hand side of Equation (5) and a forward difference to the right hand side at time level $2n+1$, then with the use of Equation (4) the result may be rearranged to yield,

$$P_{J,i,2n+1} = \frac{1}{1+C}P_{J-1,i,2n+1} + \frac{C}{1+C}P_{J+1,i,2n+1} \tag{17}$$

where,

$$j = J$$

$$i = 1, 2, 3, \ldots I$$

Alternating Direction Technique: r-Implicit Equation for the Capillary

For time level $2n+2$, Equation (7) was differenced again, in a reverse manner, by replacing the r-derivatives with an implicit formulation and the X-derivatives with an explicit formulation. Substituting the differenced forms into Equation (7), collecting terms and rearranging yields,

$$F_j'P_{j+1,i,2n+2} + G_j'P_{j,i,2n+2} + H_j'P_{j-1,i,2n+2} = Z_j' \tag{18}$$

where,

$$j = 2, 3, 4, \ldots J-1$$

$$i = 2, 3, 4, \ldots I$$

Notice that in this case the term $K_{j,i,2n+1}$ requires the value of $P_{j,i,2n+1}$ and not $P_{j,i,2n+2}$. Since $P_{j,i,2n+1}$ is known from solution of the X-implicit equations, there was no need in the r-implicit solution for a special equation to treat the nonlinearity. As a result the terms F', G' and H' were readily obtained for each j row, and the Z' terms were easily determined by use of boundary condition 1 and known values of the dependent variable at time level $2n+1$.

Combining boundary condition 3 with the fictitious boundaries, the following equalities are valid:

$$P_{1,i,2n+2} = P_{2,i,2n+2} \qquad 1 \leq i \leq I \tag{19}$$

In addition if we let,

$$\begin{aligned} P_j &= P_{j,i,2n+2} \\ P_{j+1} &= P_{j+1,i,2n+2} \\ P_{j-1} &= P_{j-1,i,2n+2} \end{aligned} \tag{20}$$

and apply Equation (19) to Equation (18), the following set of equations applies to each i row within the capillary:

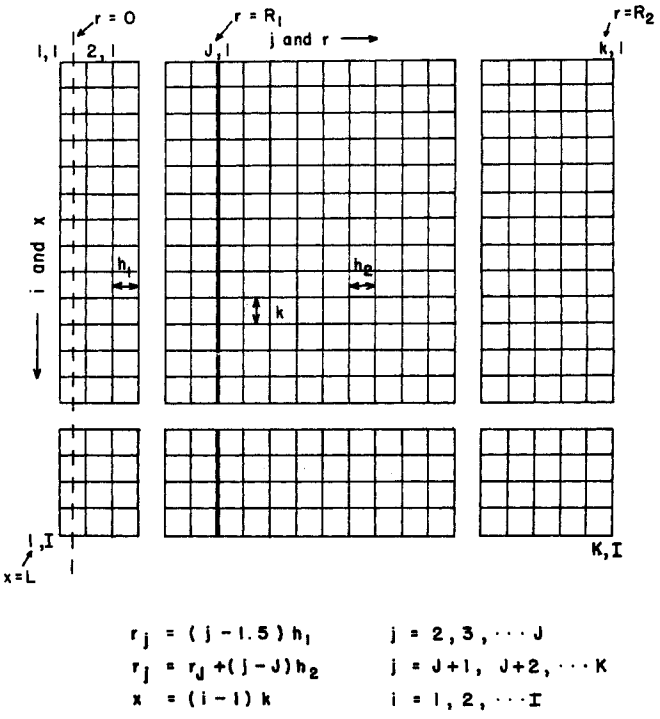

Fig. 4. Gridwork of the capillary tissue system of the cross section from $r = 0$ to R_2 and $x = 0$ to $x = L$.

$$(G_2' + H_2')\, P_2 + F_2' P_3 = Z_2' \qquad j = 2$$
$$H_j' P_{j-1} + G_j' P_j + F_j' P_{j+1} = Z_j' \qquad 3 \leq j \leq J-1 \tag{21}$$

Although Equation set (21) applies to each i row bounded by $2 \leq i \leq I$ and $2 \leq j \leq j-1$, it cannot be solved without further information concerning the interface and tissue.

Alternating Direction Technique: r-Implicit Equation for the Tissue

Equation (6) was implicitly differenced with respect to the r-direction in the same manner as the capillary equation. The resulting algebraic equation was,

$$FF_j'\, P_{j+1,i,2n+2} + GG_j'\, P_{j,i,2n+2} + HH_j'\, P_{j-1,i,2n+2} = ZZ_j' \tag{22}$$

where,

$$j = J+1, J+2, \ldots K$$
$$i = 1, 2, 3, 4, \ldots I$$

The constants FF_j', GG_j', and Z_j' were calculated with use of known values of the dependent variable on time level $2n+1$ and boundary condition 2 and 5.

In accordance with boundary condition 4,

$$P_{K+1,i,2n+2} = P_{K-I,i,2n+2} \tag{23}$$

Substituting Equation (23) into Equation (22) and applying the terminology established in Equation (20), the following is attained for each i row:

$$HH_j'\, P_{j-1} + GG_j'\, P_j + FF_j'\, P_{j+1} = ZZ_j' \qquad J+1 \leq j \leq K-1$$
$$(HH_K' + FF_K')\, P_{K-1} + GG_K'\, P_K = ZZ_K' \qquad j = K \tag{24}$$

Equation set (24) is valid for each i row bounded by $1 \leq i \leq I$ and $J+1 \leq j \leq K$ but cannot be solved without additional information concerning the interface and capillary.

Interface Equation for Use with the r-Implicit Capillary and Tissue Equations

Conditions at the interface cannot be calculated the same way as in the X-implicit scheme because positions $J+1$ and $J-1$ at time level $2n+2$ are not known. Therefore, rewriting Equation (17) for time level $2n+2$ yields,

$$FI'P_{J+1,i,2n+2} + GI'P_{J,i,2n+2} + HI'P_{J-1,i,2n+2} = 0 \tag{25}$$

where,

$$j = J$$
$$i = 1, 2, 3, \ldots I$$

Combination of r-Implicit Equation Sets

For the $i = 1$ row, if boundary condition 1 is applied to interface Equation (25) and the results incorporated into tissue Equation set (24), the following set is obtained:

$$GI'\, P_J + FI'\, P_{J+1} = HI'\, P_{J-1} \qquad j = J$$
$$HH'_j\, P_{j-1} + GG'_j\, P_j + FF'_j\, P_{j+1} = ZZ'_j \qquad J+1 \leq j \leq K-1$$
$$(HH'_K + FF'_K)\, P_{K-1} + GG'_K\, P_K = ZZ'_K \qquad j = K \tag{26}$$

Equation set (26) allows the values of the dependent variable at $i = 1$ for time level $2n+2$ to be calculated by the method of Thomas (7).

A combination of capillary Equation set (21) interface Equation (25) and tissue Equation set (24) yields,

$$(G'_2 + H'_2)\, P_2 + F'_2\, P_3 = Z'_2 \qquad j = 2$$
$$H'_j P_{j-1} + G'_j P_j + F'_j P_{j+1} = Z'_j \qquad 3 \leq j \leq J-1$$
$$HI' P_{J-1} + GI' P_J + FI' P_{J+1} = 0 \qquad j = J$$

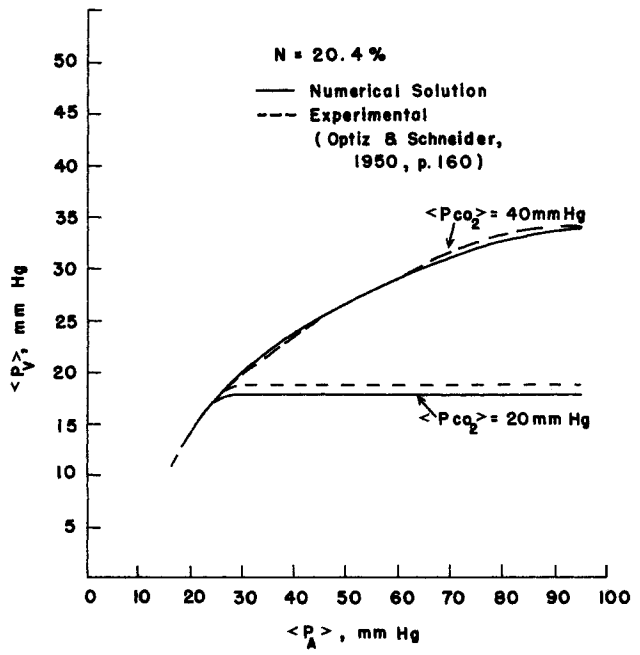

Fig. 5. Comparison plot of arterial oxygen partial pressure of the capillary vs. corresponding venous partial pressure for $<P_{CO_2}> =$ 40mm. Hg. and $<P_{CO_2}> =$ 20mm. Hg.

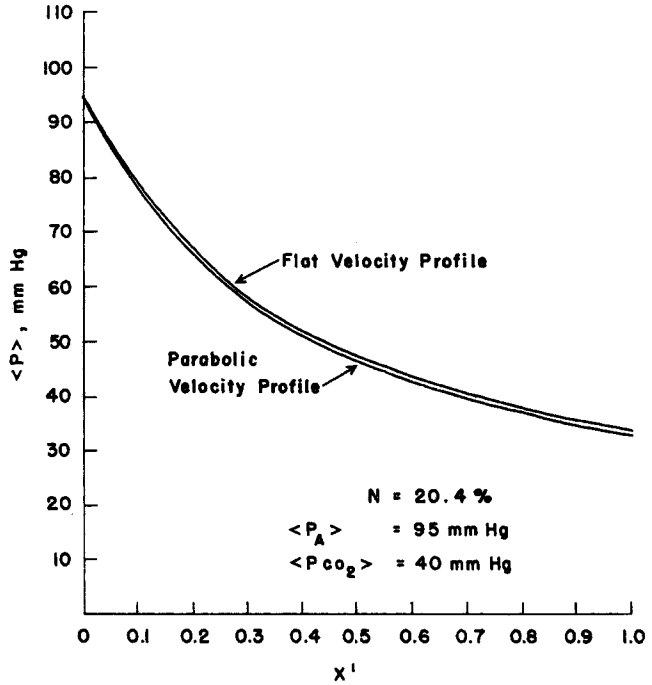

Fig. 6. Comparison of the effect produced on the axial partial pressure profile by changes in the velocity profile.

$$HH'_j P_{j-1} + GG'_j P_j + FF'_j P_{j+1} = ZZ'_j$$

$$J + 1 \leqq j \leqq J - 1 \quad (27)$$

$$(HH'_K + FF'_K)\, P_{K-1} + GG'_K P_K = ZZ'_K$$

$$j = K$$

The group of different equations fit the requirements for solution by the method of Thomas and can be applied to each i row within the range $2 \leqq i \leqq I$; $2 \leqq j \leqq K$.

Application of the Method

For $n = 0$, Equation set (13), X-implicit equations, is used to calculate the dependent variable at time level $2n + 1$. Solution is conducted by columns from $j = 2$ to $j = J - 1$. Equation set (16) calculates columns from $j = J + 1$ to $j = K$. After these columns are determined, Equation (17) is applied independently on each i row to calculate interface conditions. Initial values for known time level $2n$ are obtained from steady state solutions (*15*).

Next, for $n = 0$, Equation set (26) is used to calculate the interface and tissue conditions on the $i = 1$ row at time level $2n + 2$. Then Equation set (27), r-implicit equations, is used row by row to calculate capillary, interface, and tissue conditions at time level $2n + 2$ from $i = 2$ to $i = I$.

After the dependent variable has been determined at time level $2n + 1$ by the X-implicit equations and at time level $2n + 2$ by the r-implicit equations, n is increased by one and the above procedure repeated in order to calculate conditions at the new time levels $2n + 1$ and $2n + 2$. The cycle is repeated until a desired time level is reached.

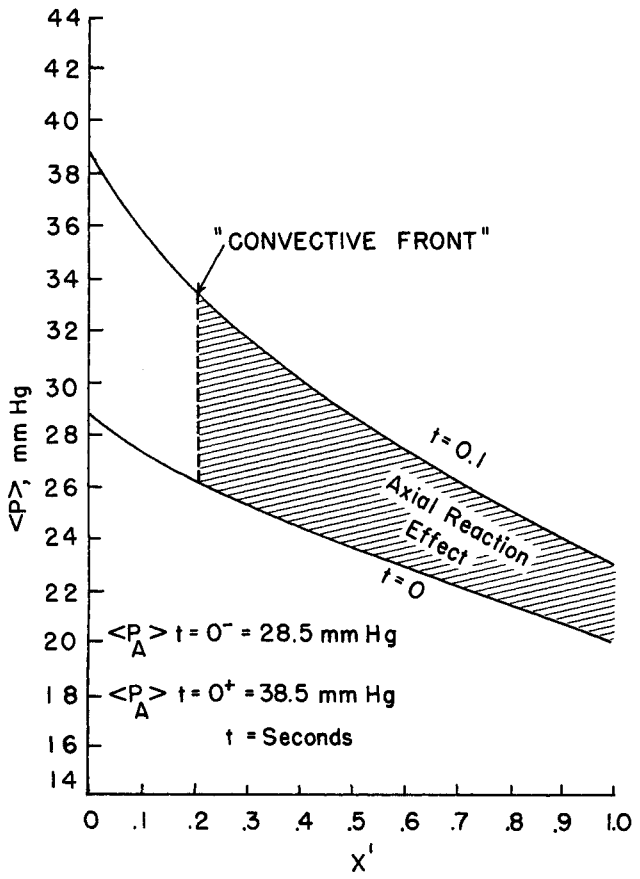

Fig. 7. Graphical demonstration of the axial reaction effect during transient changes.

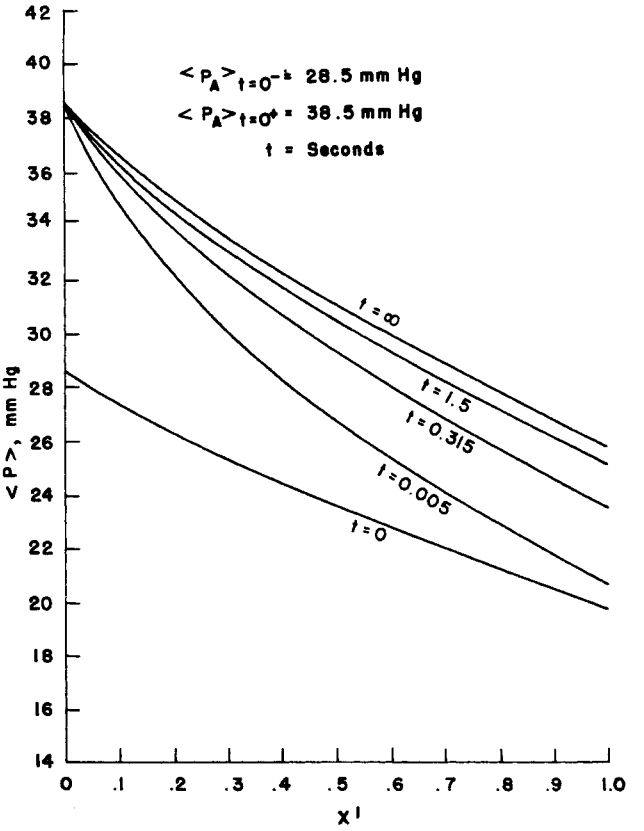

Fig. 8. Space average oxygen partial pressure axial profiles for the capillary at various times.

After several applications for the same size time increment, the magnitude of the time increment can be cautiously increased. The increase should come only after numerous calculations have been made and after the two alternating techniques have been applied an equal number of times.

Stability

Due to the complexity of the equations, mathematical proofs of the numerical solution techniques were not obtained. Likewise, it was not possible to develop equations predicting correct increment sizes. Stability and convergence were rigorously tested on the computer by trial and error selection of correct increment sizes (axial, radial, and time).

A stability limitation was reached on the magnitude of the time increment. However the upper limit was large enough to allow a successful solution.

Computer Program

The methods outlined in this section were programmed in Fortran IV and processed on an IBM 7094 digital computer. Computing continued until 80 to 90% of the total response had occurred. (This required about 10 hr. of computer time.)

DISCUSSION

The case selected for transient analysis was that of a normal person existing under alveolar oxygen conditions such that the arterial oxygen partial pressure of blood entering capillaries of grey matter was 28.5 mm. Hg. Under these conditions venous blood leaving capillaries has an oxygen partial pressure of 19 mm. Hg. and the person is in the arterial hypoxic state (*14*). Any reduction in arterial oxygen supply will cause unconsciousness.

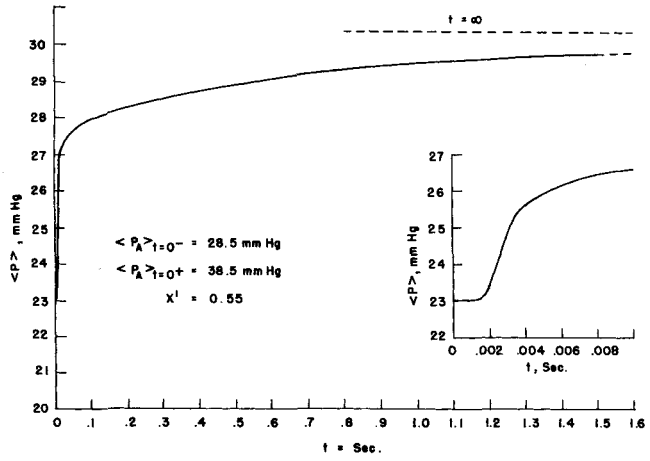

Fig. 9. Space average oxygen partial pressure time response for the capillary at $X^1 = 0.55$.

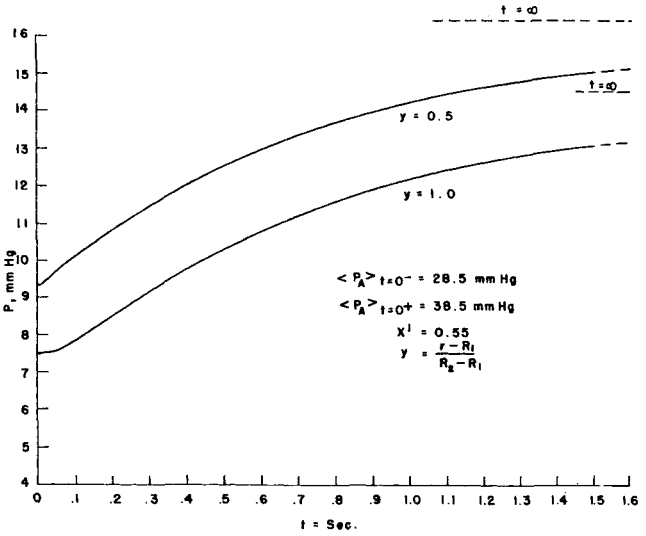

Fig. 10. Oxygen partial pressure time responses of the tissue cylinder at $X^1 = 0.55$.

An unsteady state situation was created by allowing arterial oxygen partial pressure to increase suddenly (step change) to 38.5 mm. Hg. All other factors were held constant. Transient recovery from the hypoxic condition was then obtained by the numerical solution technique. Comparative states at both $t = 0$ and $t = \infty$ were obtained from steady state solutions (*16*).

Application of a constant step change to the capillary entrance implies an infinite source is available. The rate of flow of blood through capillaries is significantly less than through arterioles, and the dimensions of capillaries are much smaller. Since capillaries branch directly from arterioles it seems reasonable to assume that an infinite source at the capillary entrance can be approached.

The diameter of the capillary (in the hypoxic state) was taken as 6.0μ (*20*) and a blood velocity of 0.04 cm./sec. was used (*16*). When using 30μ as the tissue region radially supplied by a cerebral capillary and 0.04 cm./sec. as the velocity of capillary blood, steady state material balance consideration (utilizing experimental data for normal conditions) gives a system length of 180μ (*16*).

Axial Reaction in the Capillary

The role played by axial reaction* in the capillary was of major importance in the simulation. When a step change increase of infinite supply is placed on the capillary entrance, hemoglobin in the capillary reacts rapidly (according to the distributed parameter model) and transports oxygen throughout the capillary increasing the quantity of oxyhemoglobin and plasma oxygen. The nonlinear reaction term in Equation (3) involves the expressions $VNknP^{n-1}/C_1(1 + kp^n)^2$ and $\partial P/\partial x$ which describes the axial uptake of oxygen by oxyhemoglobin when a step change in P occurs to $x = 0$. Results from the theoretical analysis showed that during the initial stages of the transient response, mass was transported down the capillary by axial reaction many times faster than by bulk capillary blood flow. The position to which mass has been moved by flow is called here the *convective front.*

Theoretically, mass could be axially transported at a rate exceeding convective flow by axial diffusion, axial reaction, or a combination of axial diffusion and axial reaction. Detailed computer solutions of the mathematical model with and without the reaction term showed clearly that the effect of axial diffusion was insignificant compared to the effect of axial reaction.

Figure 7 shows that when the convective front has moved only a part of the total axial distance, the effect of axial reaction is present throughout the capillary length. As can be seen, the increase in values is not negligible.

As time increases, the step change gradient in the axial direction becomes less severe, and the effect of axial reaction decreases. The diminishing role of axial reaction as time increases continues until a point is reached where axial reaction in the capillary is negligible. Figure 8 shows axial profiles at various times, and the asymptotic approach to $t = \infty$. Note the axial reaction effect during initial times as compared to the slow increase in values during latter times.

The impact of axial reaction on all capillary positions is notable. At all points axial reaction accomplished at least 50% of the total change before the convective front became very apparent.

Transient Response of the Capillary at Selected Axial Positions

Changes in oxygen partial pressures in the capillary as a function of time developed in two phases. First, there was a time period of rapid response but short duration; and second, a period of slow response and relatively long duration. In the second period oxygen partial pressures asymptotically approached the new steady state as time increased.

Figure 9 represents space average oxygen partial pressure time response at a selected axial position. Comparison of this figure with similar figures for different positions showed that partial pressure changes and the rate of change in the periods of rapid response are greatest at positions close to the capillary entrance. Since the magnitude of the axial gradient is largest at the capillary entrance, it is reasonable to expect a faster rate of axial reaction at small X' positions. As mass diffuses down the capillary and the axial gradient is reduced, the rate and amount of change (during initial times) is less. (See insert in Figure 9.) All rapid response periods result from axial reaction.

When convective suppy begins to dominate, time response in the capillary enters the second phase and the steady state is slowly approached. The decrease in axial reaction is not the main reason for the long, slow response period. After the initial period, the diffusion of oxygen radially outward into the tissue becomes appreciable and has a dominating effect on capillary conditions.

A time constant, τ, at a given position is defined here as

* Reaction from arterial end toward venous end of the capillary.

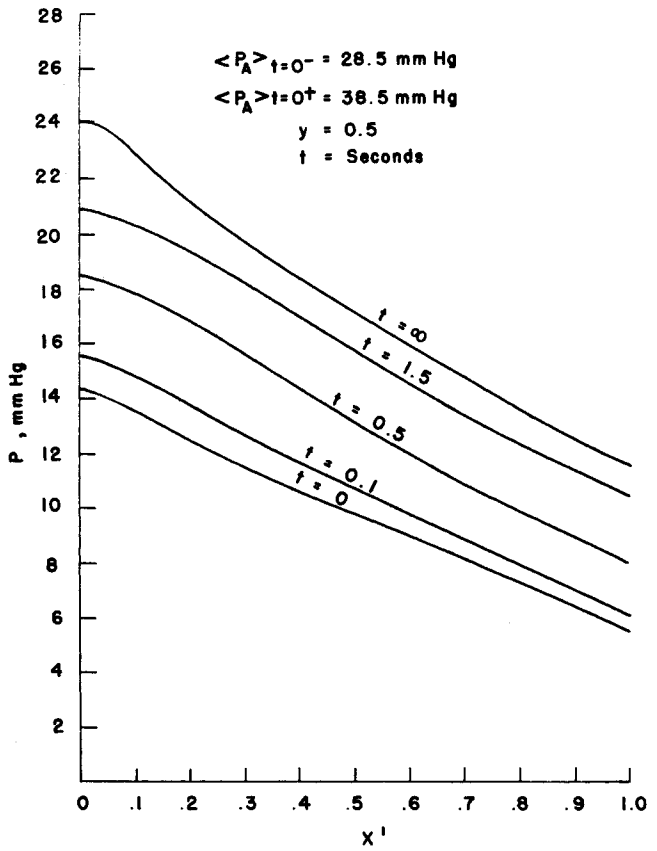

Fig. 11. Transient axial oxygen partial pressure profiles for the tissue cylinder at y = 0.5.

the time necessary for 63.2% of the total change to occur. The zero basis at each position is taken at $t = 0$ when the step change is applied to the capillary entrance. Accordingly, time constants for the capillary at axial positions 0.16, 0.55, and 1.0 were 0.0022, 0.05 and 0.33 sec., respectively.

Transient Response of the Tissue at Selected Positions

In comparison with the capillary, the transient response in the tissue is slow. Since the tissue essentially obtains oxygen only by radial diffusion from the capillary, an axial reaction effect similar to that in the capillary was not found. Consequently the phase of rapid response was not encountered, and the response curves for all tissue positions had the same damped (relative to the capillary) response appearance.

Figure 10 represents transient conditions in the tissue at one axial and two corresponding radial positions. The axial position is the same as the one given for the capillary graph, but for the axial position response curves are given for radial positions at the tissue midpoint ($Y = 0.5$) and extremity ($Y = 1.0$). Comparison with similar curves at different axial positions indicates that only a very small "transport delay" exists between tissue positions near the entrance and exit regions. In other words, appreciable quantities of oxygen begin diffusion into the tissue cylinder at all axial positions within a small time period. Since the convective front of the capillary was still in the arterial region when diffusion into tissue was first observed, oxygen for radial diffusion was initially supplied to venous capillary positions by the aforementioned axial reaction process. Thus, axial reaction in the capillary is beneficial because in initial transient stages it allows oxygen to be supplied to tissue nerve cells at the lethal corner approximately 10 times faster than the convective front. Under critical conditions this fast supply could mean the difference between nerve cell life or death.

For axial positions 0.16, 0.55, and 1.0 and radial position $Y = 0.5$, time constants are 0.74, 0.86 and 0.93 sec., respectively; and for the same axial positions, but $Y = 1.0$, the time constants are 0.85, 0.93, and 1.0 sec., respectively. It is interesting to observe that 63.2% of the total change has occurred at the lethal corner 1 sec. after the step change was applied to the capillary entrance.

Since the relative increase of oxygen in the tissue at a given radial position occurs for all axial positions at approximately equal times (compare the above time constants), axial gradients much larger than those found in the steady state were not observed. Consequently, for the conditions studied axial diffusion in the tissue was of minor importance. A slight effect was observed in the entrance region and appears in axial profile curves.

Transient Tissue Axial Profile Curve at a Selected Radial Position

Figure 11 represents axial oxygen partial pressure profiles at the tissue radial midpoint for different time levels. As expected the largest changes occurred during the earlier time periods. The difference at $X' = 0$ between the oxygen partial pressure at $t = 1.5$ and $t = \infty$ was larger than at other positions. As previously explained this is the region in which the largest total changes occur between $t = 0$ and $t = \infty$. However, it appears that as oxygen partial pressures increase with time at the $X' = 0$ position, an axial gradient sufficient for a small axial diffusion process is established. Consider the following: At time $t = 0.5$, the $X' = 0$ position of Figure 11 has completed 43% of its total change; and the $X' = 1.0$ position has increased 41% of its total change. But at time $t = 1.5$, the $X' = 0$ position has increased 67.5% of its total change and the $X' = 1.0$ position has increased 80.3%. Thus it appears that the rate of increase of oxygen at $X' = 0$ is reduced with increasing time in a greater percentage than the $X' = 1.0$ position. Since the axial gradient in the new steady state is known to be greater at $X' = 0$ than in the previous steady state, it is possible that oxygen is removed from $X' = 0$ by axial diffusion in increasing amounts as $t = \infty$ is approached.

Transient Radial Profile Curve

The transient radial profile curves presented in Figure 12 show the rapid capillary response and slower tissue response. The curves apply for axial position 0.55 but are representative of the system.

At zero time, the drop in oxygen partial pressure from the capillary center line to the capillary-tissue interface was approximately 4.8 mm. Hg. Within 0.005 sec. the radial drop in the capillary reached a maximum of 6.5 mm. Hg., and then slowly declined with time until the 4.8 mm. Hg. drop was again reached at the new steady state. The larger

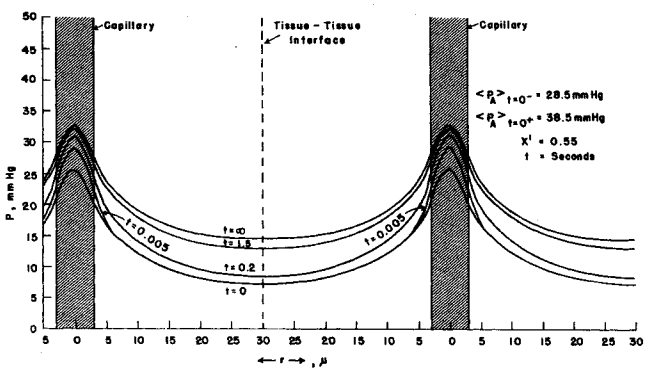

Fig. 12. Radial oxygen partial pressure profiles for the capillary-tissue arrangement at various times.

drop during the early time period was a function of the rapid increase of oxygen partial pressure through axial reaction. As the increase occurred, the radial gradient across the capillary wall increased quickly; and mass began diffusing at a faster rate into the tissue, thereby producing the larger capillary radial pressure drop. As the rate of increase in the capillary by axial reaction decreased, the gradient across the capillary wall became constant and finally decreased with increase of partial pressures in the tissue. Thus, the eventual return to the 4.8 mm. Hg. drop was accomplished.

Validity of Results and Solution Technique

As stated earlier, complete rigorous mathematical proofs for the methods developed to solve the unsteady state problem were not obtained. In the absence of experimental data, the following criteria was used to determine accuracy of results:

1. Were the solutions stable and convergent?
2. Did the solutions converge to the correct values?
3. How did the results compare with the work of previous investigators?

The solutions were stable and convergent. When correct increment sizes were found, the values did converge to the values predicted by steady state solutions (*16*).

The unusually fast response, found in this study, of the tissue to a change in capillary conditions is somewhat verified in at least one experimental study. Davies and Bronk (*8*) reported that cortex (grey matter) uses up its supply of dissolved oxygen in 0.8 sec. if the circulation is occluded locally. This record of oxygen partial pressure in the cortex of a lightly anesthetized cat was obtained with a 27 μ platinum open type electrode.

Since the models were convergent and stable, converged to predicted values, and agreed with the work of others, it seems reasonable to assume that the results and solution technique are accurate. Exact theoretical methods for determining stability and convergence for nonlinear partial differential equations of the type encountered in this work are not, to our knowledge, available at this time. Therefore, the commonly accepted increment size trial and error procedure, often used in numerical solutions, was applied.

CONCLUSIONS

On the basis of an arterial oxygen partial pressure step change the following conclusions were drawn from the solution of the distributed parameter, unsteady state model:

1. The numerical techniques derived for solution of the model were accurate.
2. For the case studied, approximately 80% of all changes between $t = 0$ and $t = \infty$ occurred in 1.5 sec.
3. During initial times, the model predicts axial reaction in the capillary and predominates over convection and molecular diffusion.

ACKNOWLEDGMENT

This work received support from a National Defense Education Act Fellowship, United States Public Health Service Fellowship 1-F1-GM-33, 804-01, and United States Public Health Service Grants 1 R01 B06957-01 NEUB, HE-04176, HE-05340 and HE-07114. Special acknowledgment goes to Mr. Daniel Sheehen, Associate Director, and Dr. James Carmon, Director, University of Georgia Computing Center, for making available the IBM-7094 digital computer and giving valuable assistance in program preparation and computation.

NOTATION

A = constant metabolism of grey matter, cc. oxygen/cc. tissue-sec.
C = $D_2\, c_2 h_1 / D_1 c_1\, h_2$
c_1 = oxygen solubility coefficient for blood, cc. oxygen/cc. blood-mm. Hg.
c_2 = oxygen solubility coefficient for tissue, cc. oxygen/cc. tissue-mm. Hg.
D_1 = oxygen diffusivity in blood, sq.cm./sec.
D_2 = oxygen diffusivity in tissue, sq.cm./sec.
e = magnitude of time increment, sec.
h_1 = magnitude of tissue radial increment, cm.
h_2 = magnitude of tissue radial increment, cm.
k = constant whose value depends on blood pH
L = length of the capillary-tissue cylinder, cm.
m = slope $\partial P/\partial x$ at $X = L$
N = combined oxygen capacity of blood, cc. oxygen/cc. blood
P = oxygen partial pressure, mm. Hg.
$\bar{P}$ = space average oxygen partial pressure, mm. Hg.
$\langle P_A \rangle$ = space average arterial oxygen partial pressure, mm. Hg.
$\langle P_V \rangle$ = space average venous oxygen partial pressure, mm. Hg.
r = radial direction, cm.
R_1 = radius of the capillary, cm.
R_2 = radius of the tissue, cm.
t = time, sec.
X = axial direction, cm.
X' = dimensionless axial length, X/L
y = dimensionless radial distance in the tissue cylinder, $r - R_1/R_2 - R_1$
η = constant whose value depends on blood pH
τ = time constant, sec.
Ψ = fractional saturation of blood with combined oxygen

LITERATURE CITED

1. Ananthakrishnan, V., W. N. Gill, and Allen J. Barduhn, *AIChE J.*, **11**, 1063 (1965).
2. Bailey, H. R., and W. B. Gogarty, Unpublished Paper, The Ohio Oil Co., Littleton, Colo.
3. Bard, Phillip, ed, 'Medical Physiology," 11th Ed., p. 595, C. V. Mosby Co., St. Louis, Mo. (1956).
4. Bloch, E. H., *Am. J. Anat.*, **110**, 125 (1962).
5. Blum, Jackob J., *Am. J. Physiol.*, **198**, 991 (1960).
6. Brian, P. L. T., *AIChE J.*, **7**, 367 (1961).
7. Bruce, G. H., D. W. Peaceman, H. H. Rachford, and J. D. Rice, *Trans. Am. Inst. Mech. Engr.*, **198**, 991 (1960).
8. Davies, P. W., and D. W. Bronk, *Federation Proc.*, **16**, 689 (1957).
9. Douglas, J., Jr., *Pacific J. Math.*, **6**, 35 (1956).
10. ———, *Am. Math. Soc.*, **89**, 484 (1958).
11. Hill, A. V., *Proc. Roy. Soc., B* **104**, 39-96 (1928).
12. Kety, Seymour S., *Federal Proc.*, **16**, 666 (1957).
13. Krogh, August, "The Anatomy and Physiology of Capillaries," 1st Ed. Yale Univ. Press, New Haven, Conn. (1922).
14. Opitz, Erich, and Max Schneider, Ergeb. Physiol., biol. Chem., Expt. Pharmakol., **46**, 126 (1950).
15. Peaceman, D. W., and H. H. Rachford, Jr., *J. Soc. Ind. Appl. Math.*, **3**, No. 1, 28 (1955).
16. Reneau, D. D., D. F. Bruley, and M. H. Knisely, *Chem. Eng. Medicine Biol.*, Proc. 33rd Annual Chem. Eng. Symposium Plenum Press, Cincinnati, Ohio (1967).
17. ———, Ph.D. thesis, Clemson Univ., Clemson, S. C. (1966).
18. Roughton, F. J. W., *Proc. Roy. Soc., B*, **140**, 203 (1952).
19. ———, "The Oxygen Equilibrium of Mammalian Hemoglobin, in 'Oxygen,'" Proc. Symp. N. Y. Heart Assoc., pp. 105-126. Little, Brown and Company, Boston, Mass. (1965).
20. Thews, Gerhard, *Pflugers Archiv.*, **271**, 197 (1960).
21. Wells, Roe E., Jr., *New Eng. J. of Med.*, **270**, 832 (1964).

Manuscript received January 24, 1967; revision received June 3, 1968; paper accepted June 5, 1968. Paper presented at AIChE Houston meeting.